Acta Biomaterialia xxx (xxxx) xxx

Contents lists available at ScienceDirect

Acta Biomaterialia

journal homepage: www.elsevier.com/locate/actabiomat

Full length article

Synchrotron tomography of intervertebral disc deformation quantified by digital volume correlation reveals microstructural influence on strain patterns

C.M. Disney [a,b,*,1], A. Eckersley [b], J.C. McConnell [b], H. Geng [c], A.J. Bodey [e], J.A. Hoyland [b,f], P.D. Lee [c,d], M.J. Sherratt [b,2], B.K. Bay [g,2]

[a] Centre for Doctoral Training in Regenerative Medicine, The University of Manchester, Manchester, UK
[b] Division of Cell Matrix Biology and Regenerative Medicine, The University of Manchester, Manchester, UK
[c] Research Complex at Harwell, Rutherford Appleton Laboratory, Didcot, Oxfordshire, UK
[d] University College London Mechanical Engineering, Torrington Place, London, UK
[e] Diamond Light Source, Oxfordshire, UK
[f] NIHR Manchester Biomedical Research Centre, Manchester University NHS Foundation Trust, Manchester Academic Health Science Centre, UK
[g] School of Mechanical, Industrial and Manufacturing Engineering, Oregon State University, Corvallis, OR, United States

ARTICLE INFO

Article history:
Received 11 January 2019
Received in revised form 1 May 2019
Accepted 7 May 2019
Available online xxxx

Keywords:
Intervertebral disc
X-ray micro-tomography
Strain
Digital volume correlation

ABSTRACT

The intervertebral disc (IVD) has a complex and multiscale extracellular matrix structure which provides unique mechanical properties to withstand physiological loading. Low back pain has been linked to degeneration of the disc but reparative treatments are not currently available. Characterising the disc's 3D microstructure and its response in a physiologically relevant loading environment is required to improve understanding of degeneration and to develop new reparative treatments. In this study, techniques for imaging the native IVD, measuring internal deformation and mapping volumetric strain were applied to an *in situ* compressed *ex vivo* rat lumbar spine segment. Synchrotron X-ray micro-tomography (synchrotron CT) was used to resolve IVD structures at microscale resolution. These image data enabled 3D quantification of collagen bundle orientation and measurement of local displacement in the annulus fibrosus between sequential scans using digital volume correlation (DVC). The volumetric strain mapped from synchrotron CT provided a detailed insight into the micromechanics of native IVD tissue. The DVC findings showed that there was no slipping at lamella boundaries, and local strain patterns were of a similar distribution to the previously reported elastic network with some heterogeneous areas and maximum strain direction aligned with bundle orientation, suggesting bundle stretching and sliding. This method has the potential to bridge the gap between measures of macro-mechanical properties and the local 3D micro-mechanical environment experienced by cells. This is the first evaluation of strain at the micro scale level in the intact IVD and provides a quantitative framework for future IVD degeneration mechanics studies and testing of tissue engineered IVD replacements.

Statement of Significance

Synchrotron in-line phase contrast X-ray tomography provided the first visualisation of native intact intervertebral disc microstructural deformation in 3D. For two annulus fibrosus volumes of interest, collagen bundle orientation was quantified and local displacement mapped as strain. Direct evidence of microstructural influence on strain patterns could be seen such as no slipping at lamellae boundaries and maximum strain direction aligned with collagen bundle orientation. Although disc elastic structures were not directly observed, the strain patterns had a similar distribution to the previously reported

* Corresponding author at: C.010 George Begg Building, Manchester M1 7DN, UK.
E-mail addresses: catherine.disney@manchester.ac.uk (C.M. Disney), alexander.eckersley@manchester.ac.uk (A. Eckersley), james.mcconnell@manchester.ac.uk (J.C. McConnell), andrew.bodey@diamond.ac.uk (A.J. Bodey), judith.a.hoyland@manchester.ac.uk (J.A. Hoyland), peter.lee@ucl.ac.uk (P.D. Lee), michael.j.sherratt@manchester.ac.uk (M.J. Sherratt), brian.bay@oregonstate.edu (B.K. Bay).
[1] Present address: School of Mechanical, Aerospace & Civil Engineering, The University of Manchester, Manchester, UK.
[2] Joint senior authors.

https://doi.org/10.1016/j.actbio.2019.05.021
1742-7061/

elastic network. This study presents technical advances and is a basis for future X-ray microscopy, structural quantification and digital volume correlation strain analysis of soft tissue.

1. Introduction

Chronic low back pain which affects a large proportion of the population is associated with age-related structural changes in the degenerated intervertebral disc (IVD) [1,2]. Currently, there are no reparative treatments for IVD degeneration which is managed with symptomatic pain relief and surgery with poor outcomes of 12% requiring reoperation and over a third of which progress to lumbar fusion [3,4].

The IVD provides flexibility in the spine whilst transmitting and attenuating loads from body weight and physical activity. The nonlinear viscoelastic behaviour of the disc allows flexibility at low loads and maintains structural integrity with increasing rate and magnitude of loading [5–8]. Regional anisotropic mechanical properties transmit and distribute forces [9–12]. These unique mechanical properties are defined by the IVD's complex and multiscale extracellular matrix (ECM) structure. Yet, direct observation of IVD structural deformation under load has been limited by 2D imaging or 3D studies of small extracted samples and strain analysis methods.

Located in the centre of the IVD, the nucleus pulposus (NP) which is rich in proteoglycans, primarily aggrecan, whose hydrophilicity causes high osmotic pressure to the surrounding tissue. The NP is surrounded by the annulus fibrosus (AF); a ring of fibrocartilage with lamellar architecture. Collagen I fibres form aligned bundles which have alternating oblique orientation between adjacent lamellae (Fig. 1a) [13,14]. Between the lamellar structures there are fibrous interconnecting bridges mainly consisting of elastin [15,16]. As the spine is loaded, cartilage endplates at the vertebrae distribute the load and the hydrostatic pressure generated in the NP is transmitted to a circumferential stress in the AF [17–20]. Residual stress in the AF helps to safely distribute the high pressures from the NP [21]. Recently, detailed studies of the distribution and organisation of elastic fibres in the IVD have been used to infer their role for structural integrity and tissue mechanics [22,23].

Microstructural deformation mechanisms of the AF under tension have been observed using optical microscopy [24–26]. However, a balance must be made between sample interaction and compromising native mechanics when studying microstructural deformation of a tissue [27]. These studies were 2D and required segments of tissue to be dissected, which means that it is not possible to characterise 3D tissue structure and observe deformations outside of the imaging plane. Furthermore, the tissue should be intact to preserve residual strain for physiological loading conditions [21] and forces from surrounding tissue such as ligaments [28]. Magnetic resonance imaging (MRI) has been used to map strain in an intact disc but resolution was limited (~200 μm) and unable to resolve the disc's multiscale hierarchical structure of lamellae, collagen bundles and fibrils, and therefore unable to map strain at microscale resolution [9,29]. More recently the 3D microstructure of ovine IVD was successfully reconstructed using ultrahigh field MRI (100 μm resolution) [30,31].

X-ray micro-tomography (μCT) has been used for 3D characterisation of the IVD with the use of contrast agents [32,33] but microstructure characterisation was limited. Recent advances in μCT imaging have meant it is possible to image the 3D microstructure of native soft tissues [34,35]. Soft tissues are challenging to image using μCT as they weakly absorb X-rays and they exhibit stress relaxation during long scans (hours for laboratory sources) where microstructure may move, resulting in image artefacts [36]. In-line phase contrast imaging can resolve structures in soft tissue due to variations in X-ray refractive index which alter the wave front and, with sufficient propagation past the sample, Fresnel fringes occur giving contrast enhancement at the edges of structures [37–40]. A high flux source, such as synchrotron, reduces overall scan time due to shorter exposures meaning that motion artefacts from tissue stress relaxation are lessened.

The objective of this study was to use synchrotron μCT (synchrotron CT) with in-line phase contrast to resolve the native structure of an intact IVD inside a spine segment and quantify microstructural deformation under applied sequential compression. Importantly, this provides the first direct observation of AF microstructural deformation in an intact IVD which includes the mechanical influence of surrounding spinal tissues. Three-dimensional quantification of AF deformation using digital volume correlation offers analysis of how strain is transferred through native tissue and the cellular environment. The novel imaging and strain analysis presented here builds on inferences from 2D techniques and 3D studies of small extracted samples concerning structural characterisation and IVD mechanical function. It is hoped that future application of these methods and detailed observations will help predict the likely mechanical causes of IVD degeneration and positively impact on the design and testing of tissue engineered IVD replacements [41,42] with a wider impact on soft tissue biomechanics studies.

2. Materials and methods

2.1. Tissue and materials

Retired Sprague-Dawley rats (8 week-old, male) from the University of Manchester Biological Services Facility were culled by carbon dioxide inhalation following the University's Animal Research Policy and the UK Animal (Scientific Procedures) Act 1986. The lumbar spine was dissected *en bloc*, snap frozen and stored at −80 °C. Spines were thawed before using a high precision diamond cutting blade (Accumtom-50; Struers, UK) to dissect lumbar segments (L2/L3, L3/L4) by cutting through the vertebral bodies. A slow feed speed (0.01 mm/s) and rotation blade speed (1500 rpm) with water cooling was used to minimise potential damage to the sample. Excess muscle tissue was removed from the spine segments, leaving a thin layer of muscle and ligaments intact. This layer of tissue was left intact to prevent the IVD from drying. Samples had approximate dimensions of 10 mm height, 12 mm circumference (IVD 1 mm and 6 mm respectively), were then set in a customised sample holder using non-exothermic epoxy resin (Ultra Repair; Loctite, UK).

2.2. Equipment and testing

An *in situ* compression stage Deben CT5000 (Deben, UK) with a 500 N load cell provided precise displacement control (300 nm resolution) with force readout (accuracy 1% of full scale range). Custom machined sample holders aided sample alignment. Samples were held under cumulative compression using the bottom plate. A 1 N preload (~1/3 of the animal's body weight) was applied to ensure the sample was securely in place. The compression was held for 20 min to account for tissue stress relaxation. A stress relaxation period was required so that the sample did not move

Please cite this article as: C. M. Disney, A. Eckersley, J. C. McConnell et al., Synchrotron tomography of intervertebral disc deformation quantified by digital volume correlation reveals microstructural influence on strain patterns, Acta Biomaterialia, https://doi.org/10.1016/j.actbio.2019.05.021

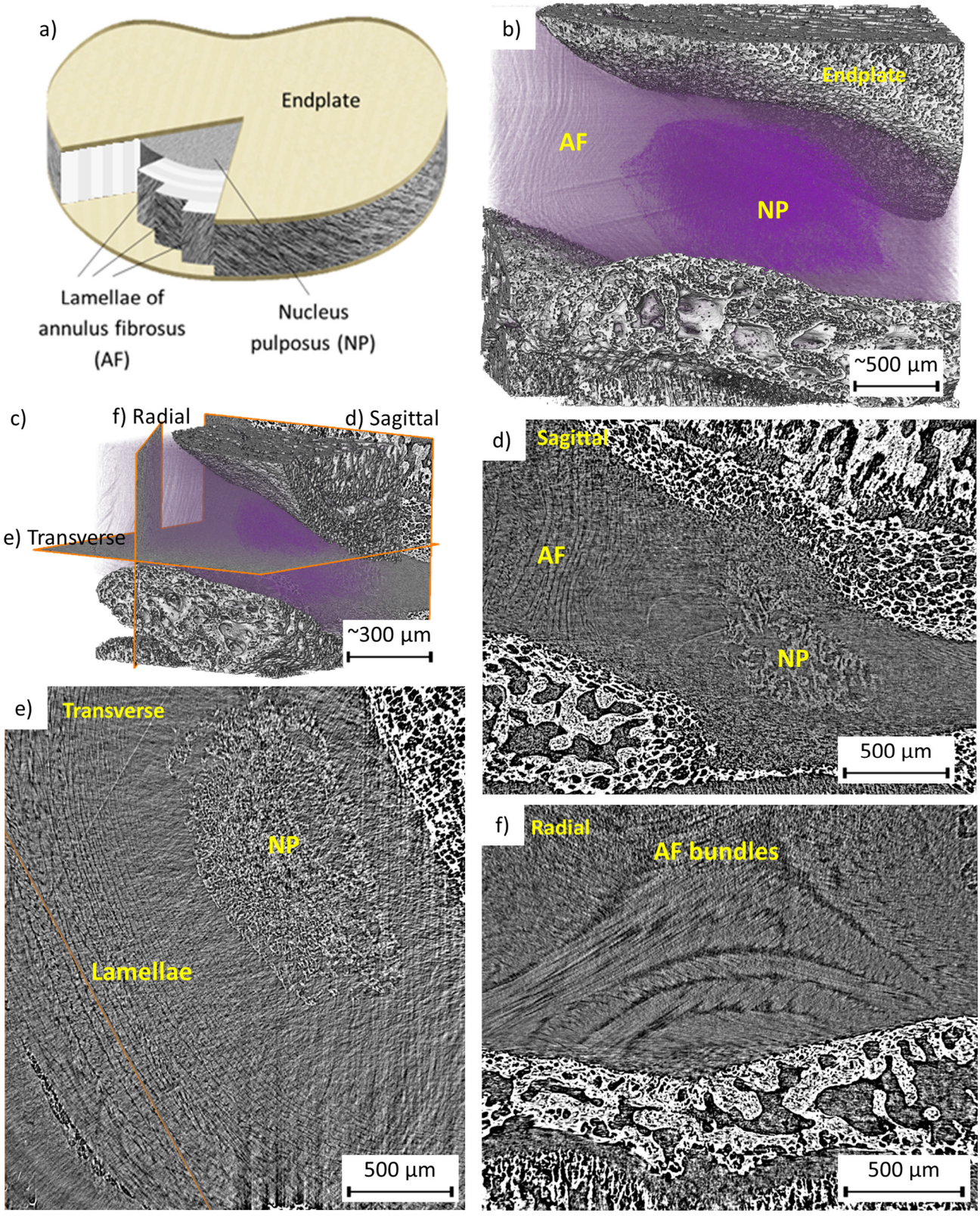

Fig. 1. Structure of native intervertebral disc; a) schematic of the IVD, b) rendered tomogram, c) virtual slices taken from three anatomical positions, d) sagittal, e) transverse and f) radial.

during the scan. A slow strain rate of 0.00167 strain/s (0.1 mm/min) was used during compression to minimise peak force response and stress relaxation time. Two scans were taken at this reference load (D0). The sample was then compressed by 0.02 mm (2% strain) displacement and 12 min allowed for stress relaxation before scanning (D1). The 2% strain compression, stress relaxation period and scanning were repeated a further 3 times (D2–D4). The compression stage recorded the force throughout

Please cite this article as: C. M. Disney, A. Eckersley, J. C. McConnell et al., Synchrotron tomography of intervertebral disc deformation quantified by digital volume correlation reveals microstructural influence on strain patterns, Acta Biomaterialia, https://doi.org/10.1016/j.actbio.2019.05.021

the experiment which showed the stress relaxation of the tissue during compression before scanning (Fig. 2a).

2.3. In-line phase contrast synchrotron micro-tomography

The Diamond-Manchester Branchline I13-2 [43,44] at Diamond Light Source was used to acquire native rat lumbar IVD synchrotron micro-tomographic data (synchrotron CT). Compared with micro-focus tube sources, synchrotron radiation has high flux, high coherence and allows large propagation distances and is able to resolve native soft tissue microstructures using in-line phase contrast techniques. Pink beam (8–30 keV) with an undulator gap of 5 mm was filtered (1.34 mm pyrolytic graphite, 3.2 mm aluminium, 0.14 mm iron) to reduce beam damage. Dose during alignment was minimised by firstly using a laser (rather than X-rays) with manual adjustments of the sample holder on the beamline, and then using projections under lowered dose conditions (large undulator gap and use of slits).

Imaging was conducted at 4 × total magnification with a pco. edge 5.5 (PCO AG, Germany) detector (sCMOS sensor of 2560 × 2160 pixels), using a 2 × objective coupled to a 500 µm $CdWO_4$ scintillator, mounted ahead of a second 2× lens. This gave a field of view of 4.2 × 3.5 mm (effective pixel size 1.625 µm) that encompassed the entire width of the sample. Exposure time for each projection was set to 0.15 s, giving ~50% saturation in flat-field images. A total of 8001 projections were recorded over 180° continuous rotation ('fly scan') to provide a high signal:noise reconstruction [45]. The last image was not used for reconstruction, but was compared to the first to check for sample deformation, bulk movements and beam damage. Propagation (sample-to-scintillator) distance was set to 500 mm which was chosen by increasing in 100 mm increments until there was sufficient in-line phase contrast to resolve the IVD microstructure. Scans were performed after sample compression and stress relaxation (Fig. 2). The projections were reconstructed with dark- and flat-field correction and ring artefact suppression using the Diamond Light Source software DAWN [46,47].

2.4. Image processing and DVC analysis

Contrast range was adjusted to minimum and maximum grey values of IVD structures. Light median filtering (1 pixel radius) was used to remove noise. Avizo 8.0 (FEI Visualization Sciences Group, Mérignac Cedex, France) was used to visualise and render the image data. For renderings in Figs. 1 and 2, endplates and IVD were segmented based on grey level and the IVD colour map was chosen to be semi-transparent so that internal structures could be seen. Two cube volumes were selected from the AF for analysis (Fig. 3a–c).

Bundle orientation in both cubes was analysed using the XFiber Extension in Avizo 8.0 [48,49]. Cylinder Correlation (length 40 pixels, angular sampling 5°, mask of 10 pixels and 8 pixels outer radius) was used to enhance fibre-like structures. Fibres were traced from initial seed points above correlation coefficient of 40 (>30 to continue tracing). A low (0.2) direction coefficient and 30° search angle was chosen to trace straighter structures and results filtered to have a minimum fibre length of 20 pixels. Orientation of each traced structure is given by theta (θ), angle with the *z* axis, and phi (φ), angle in the *x*-*y* plane. Orientation angle was transformed to the lamella-local coordinate system (Fig. 3d) and plotted as a histogram (Fig. 4).

Displacement of structures between images was tracked using digital volume correlation (DVC) Collaborative Computational Project in Tomographic Imaging (CCPi) supported code [50,51]. Point locations were set up for the centres of sub-volumes which were independently tracked between consecutive image volumes in 6 degrees of freedom (3 translation and 3 rotation) by optimisation of the normalised sum of squared difference function. DVC was conducted with high-performance cubic spline interpolation allowing displacement measurement to sub-voxel precision. Tricubic interpolation of the grey-level values with 2500 points in each sub-volume was found to be a sufficient number of points. Preliminary analysis with a smaller number of sub-volumes (1000 s) and different sub-volume sizes showed that 20 pixels (Fig. 5a) had reliable tracking whilst maintaining high tracking resolution for the AF. Points (~133,000) were evenly distributed throughout the cube

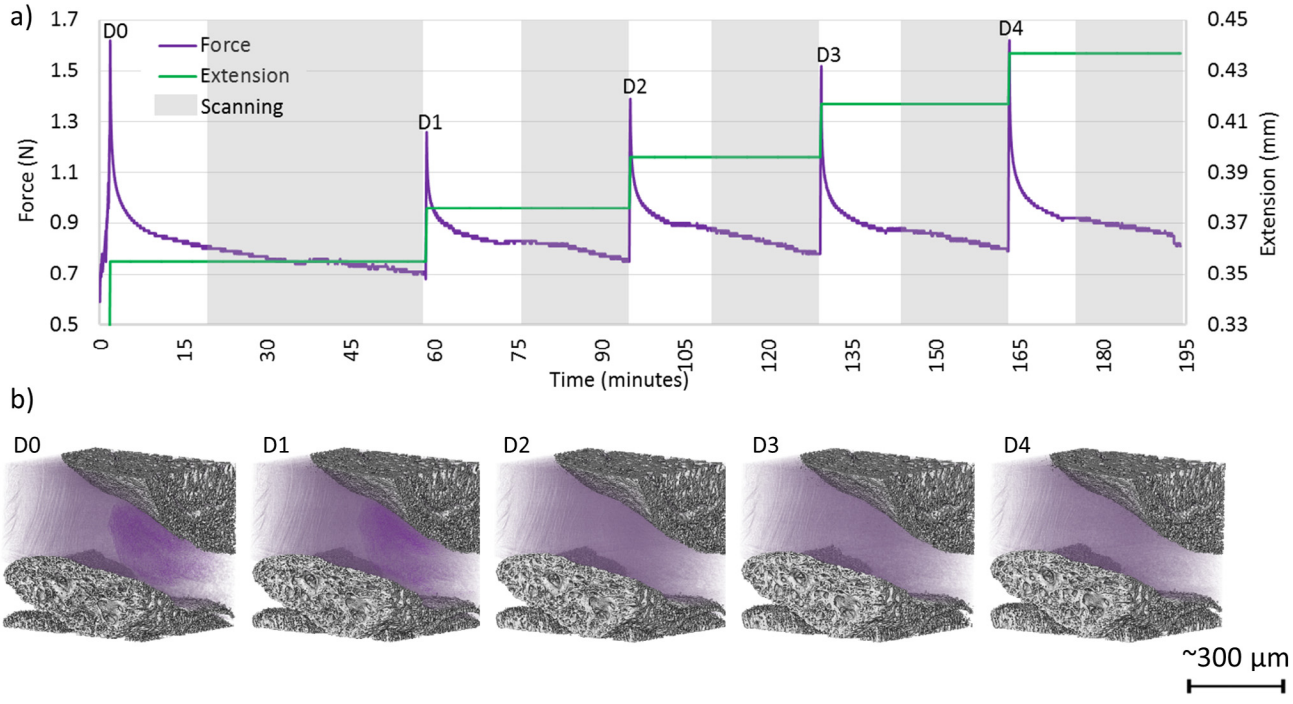

Fig. 2. *In situ* loading; a) force reading from sequential compression, b) sequence of 3D renders of the disc being compressed from the lower endplate.

Please cite this article as: C. M. Disney, A. Eckersley, J. C. McConnell et al., Synchrotron tomography of intervertebral disc deformation quantified by digital volume correlation reveals microstructural influence on strain patterns, Acta Biomaterialia, https://doi.org/10.1016/j.actbio.2019.05.021

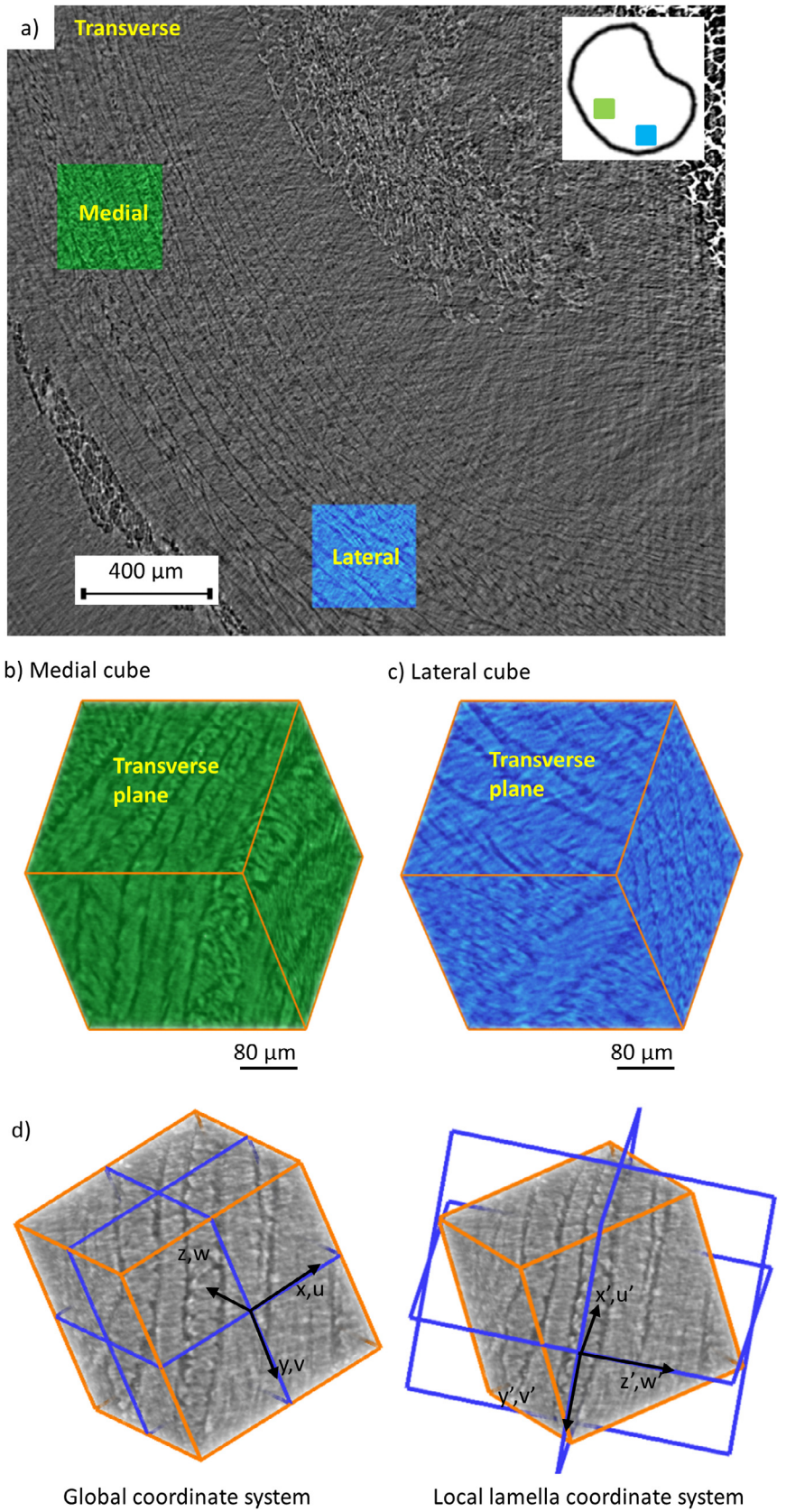

Fig. 3. Volumes of interest selected for analysis and defining a local coordinate system: a) transverse slice showing position of medial and lateral cube volumes, b) rendered medial cube, c) rendered lateral cube and d) global and local lamella coordinate system.

Please cite this article as: C. M. Disney, A. Eckersley, J. C. McConnell et al., Synchrotron tomography of intervertebral disc deformation quantified by digital volume correlation reveals microstructural influence on strain patterns, Acta Biomaterialia, https://doi.org/10.1016/j.actbio.2019.05.021

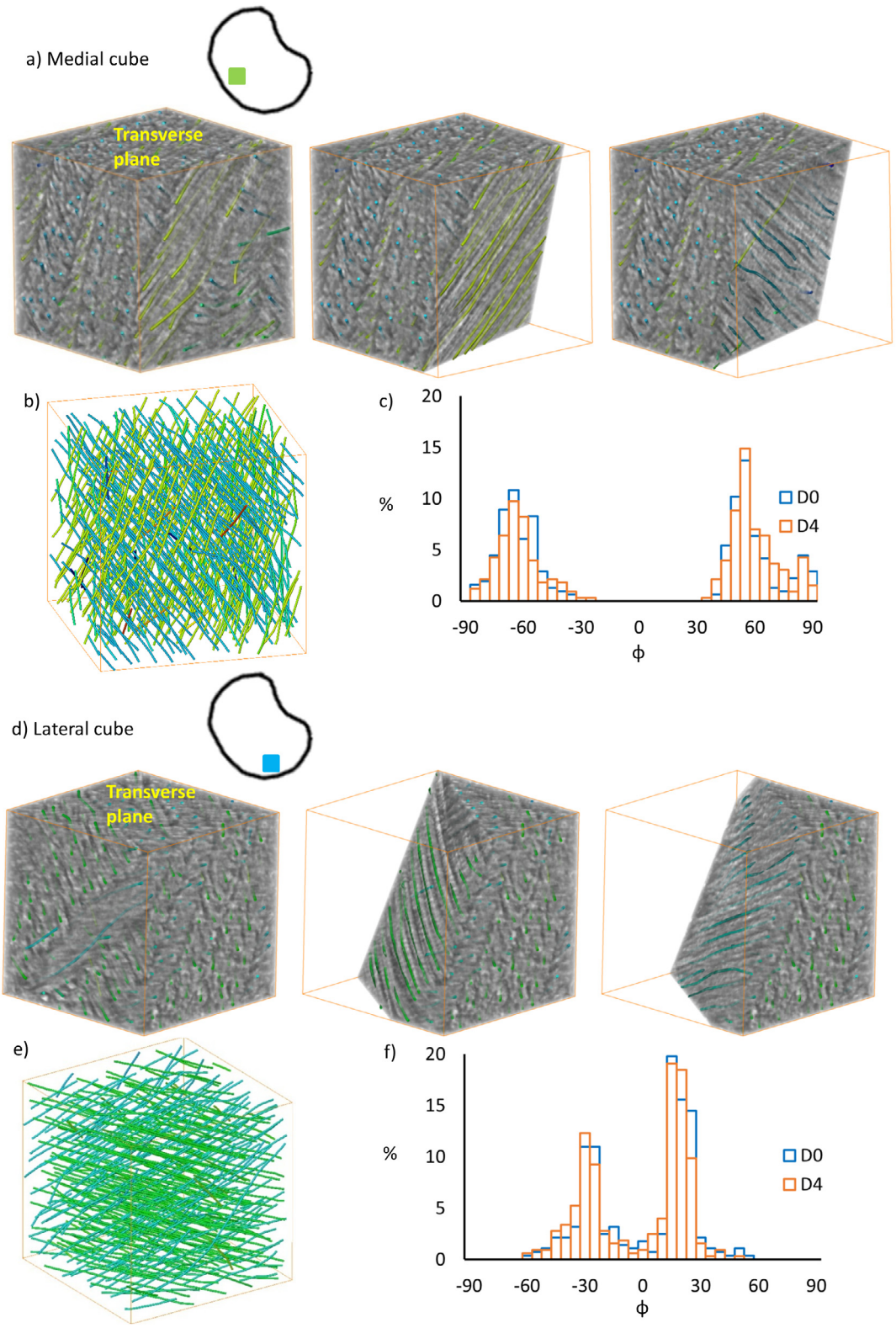

Fig. 4. Bundle orientation varies with anatomical location: a, d) two alternating orientations of collagen bundles shown by clipping in the lamella plane, b, e) all traced bundles are shown with view in lamella plane, and c, f) bundle orientation for D0 and D4 after rotation transformation to lamella local coordinate system where phi φ is in-plane angle. a–c) shows medial volume of interest, d–f) shows lateral volume of interest. Cube volumes have 320 μm dimensions.

volumes with average spacing of 4 pixels (Fig. 5b). The displacements were then added onto the original positions of each sub-volume and the process repeated for the next compression steps. DVC between the two scans at D0 serves to test the validity of the analysis. The second scan at D0 was then used as the reference for the compression sequence.

Please cite this article as: C. M. Disney, A. Eckersley, J. C. McConnell et al., Synchrotron tomography of intervertebral disc deformation quantified by digital volume correlation reveals microstructural influence on strain patterns, Acta Biomaterialia, https://doi.org/10.1016/j.actbio.2019.05.021

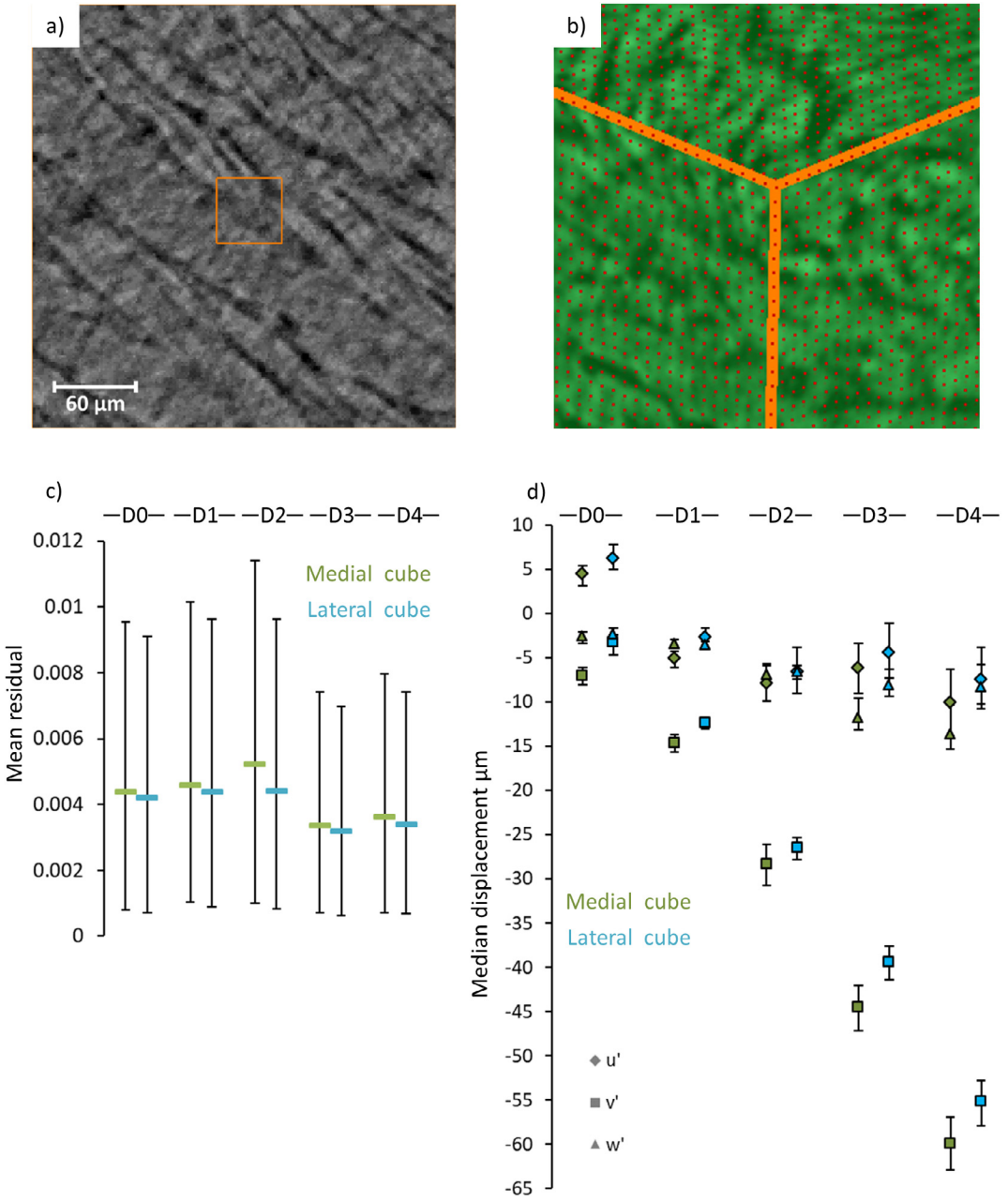

Fig. 5. Tracking displacement using DVC: a) sub-volume used for tracking was a 20 pixel (32 µm) cube shown by the orange box on the image data, b) tracking points had a 4 pixel (6.4 µm) spacing, c) mean and standard deviation of tracking residual for all compression steps, and d) median and interquartile range for displacement values in the local lamella coordinate system. (For interpretation of the references to colour in this figure legend, the reader is referred to the web version of this article.)

2.5. Transformation to local coordinates and strain calculation

Displacement data was transformed using an angle-axis rotation in Avizo to a local coordinate system so that lamellae bundles were in the *x-y* plane (Fig. 3d). Strain was calculated using MATLAB R2018a (Mathworks Inc., Natick, Massachusetts, USA). The displacement vectors were interpolated (natural) to a regular-spaced grid of 3 pixels, a median filter was applied to remove outliers followed by Gaussian as a low-pass filter (both with 3,3,3 neighbourhood). The displacement gradient (1) across the image volume was calculated to find the Lagrangian finite strain tensor (2) for each location.

$$\mathcal{D} = \begin{bmatrix} \frac{\partial u}{\partial x} & \frac{\partial u}{\partial y} & \frac{\partial u}{\partial z} \\ \frac{\partial v}{\partial x} & \frac{\partial v}{\partial y} & \frac{\partial v}{\partial z} \\ \frac{\partial w}{\partial x} & \frac{\partial w}{\partial y} & \frac{\partial w}{\partial z} \end{bmatrix} \quad (1)$$

$$\mathcal{L} = \frac{1}{2}[\mathcal{D} + \mathcal{D}^T + \mathcal{D}^T\mathcal{D}] \quad (2)$$

Eigenvectors and values gave the maximum principle vectors and strain which were saved as 32-bit unsigned images for visualisation.

2.6. Statistical analysis

Mean and standard deviation of bundle reorientation was calculated for single lamellae. Mean and standard deviation of DVC tracking residual was calculated and displayed in Fig. 5c. Median and interquartile range was calculated for DVC displacement values in Fig. 5d.

Please cite this article as: C. M. Disney, A. Eckersley, J. C. McConnell et al., Synchrotron tomography of intervertebral disc deformation quantified by digital volume correlation reveals microstructural influence on strain patterns, Acta Biomaterialia, https://doi.org/10.1016/j.actbio.2019.05.021

3. Results

3.1. Synchrotron micro-tomography of native IVD within the spine segment

Using in-line phase contrast synchrotron micro-tomography (synchrotron CT), the structure of native IVD within a spine segment was resolved, with overall structure presented in Fig. 1b. The porous endplates are mineralised and as such absorb X-rays meaning that they were readily resolved. The non-mineralised AF and NP are weakly X-ray attenuating and thus were resolved by increasing structure edge contrast using in-line phase contrast techniques. Virtual slices can be taken from any location in the volume to show their 3D structural organisation (Fig. 1c). A central region with higher grey values and fibres organised radially outwards indicates the NP which is surrounded by the lamella AF structure (Supplementary Fig. 1). A sagittal slice shows the thickness of the disc with lamellae running from the upper endplate to the lower endplate (Fig. 1d). Transverse slices show concentric layers of the AF around the NP (Fig. 1e). A radial slice reveals the structure within lamellae where there is an alternating orientation of collagen bundles (Fig. 1f).

3.2. In situ loading; tomography after stress relaxation

IVD structures were resolved in a series of time lapse scans during compression of the spine segment. As expected, samples had a viscoelastic stress relaxation response to each cumulative compression step with an initial force peak which decreased over time (Fig. 2a). The scans were taken after stress relaxation (12 minutes) and showed no movement or slipping of the sample in the holder. The IVD was compressed from the bottom endplate with minimal bending (Fig. 2b, Supplementary Video 1). Contrast in the NP decreased and an increasing number of streaking artefacts were present from the highly absorbing endplate after each compression step.

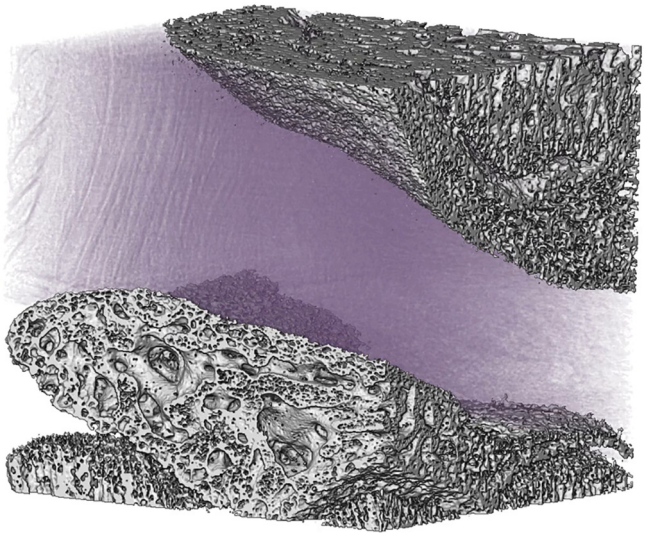

Video 1. Sequence of 3D renders of a rat spine segment being compressed from the lower endplate.

3.3. Lamellae bundle angle

Two cube volumes from different anatomical areas (Fig. 3a–c) were chosen for bundle analysis at 'zero' compression (D0) and the final compression step (D4). The alternating orientation of lamellae bundles could be observed and extracted using fibre tracing analysis (Fig. 4, Supplementary Videos 2 & 3). Bundle orientation can be compared between the two volumes after transformation to a local coordinate system where φ is the angle in the lamella plane measured from the horizontal axis. A bi-modal distribution centred roughly at 0° was shown for both volumes (Fig. 4c & f). The two peaks for the medial cube indicated a steeper inclination (55° and −65°) when compared to the lateral cube (20° and −30°). Fig. 4c & f do not show a notable change in bundle angle after sample compression. However, when average orientation of separate lamella were taken, bundles reoriented by 0.9° ± 0.4°.

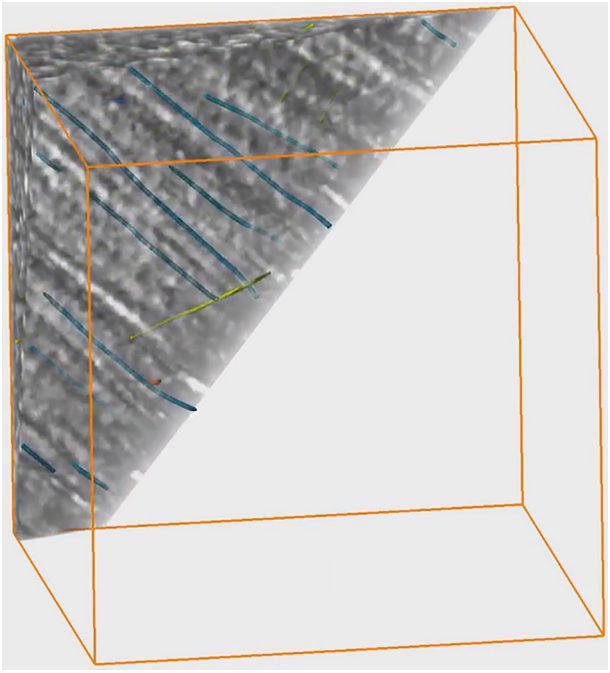

Video 2. AF collagen bundles traced in the medial volume of interest (cube with 320 μm dimensions).

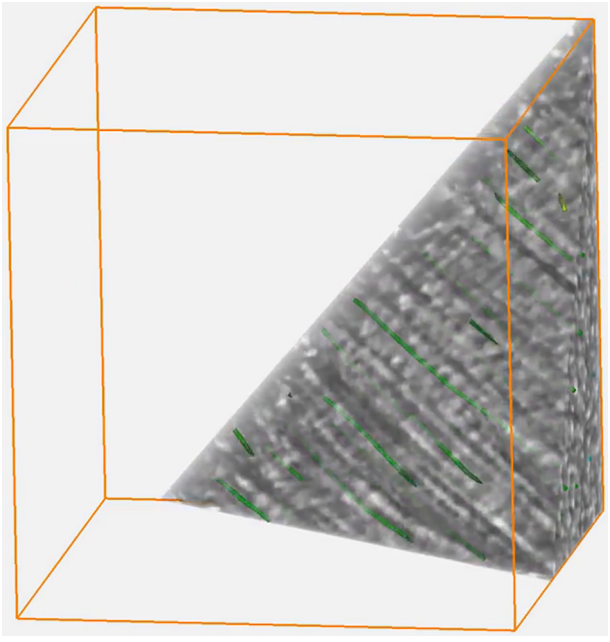

Video 3. AF collagen bundles traced in the lateral volume of interest (cube with 320 μm dimensions).

Please cite this article as: C. M. Disney, A. Eckersley, J. C. McConnell et al., Synchrotron tomography of intervertebral disc deformation quantified by digital volume correlation reveals microstructural influence on strain patterns, Acta Biomaterialia, https://doi.org/10.1016/j.actbio.2019.05.021

3.4. Digital volume correlation: displacement of structures can be tracked and mapped as strain

An overview of the image processing and DVC-based strain results are shown in Supplementary Video 4. Evenly distributed points within the two cube volumes were tracked using DVC (Fig. 5b) with an overall mean tracking residual of 0.0042 for the medial cube and 0.0038 for the lateral cube. Mean tracking residual and standard deviation are shown in Fig. 5c. Residual values do not increase or change distribution in comparison with the repeat scan (D0). Median displacement relative to the local coordinate system of each cube is plotted in Fig. 5d and interquartile range marked with error bars. There is a relatively low magnitude for lower loads which gradually increases for higher loads, moving out of the range of the repeat scan. The difference between displacement directions shows the anisotropic mechanical behaviour of the AF. The radial displacement (w') shows that the AF bulges outwards with increasing load. Highest displacement is in the loading direction (v') whilst the greatest variation (interquartile range) is in the horizontal direction of lamellae plane (u'). Note, these displacement values are relative to the original image data and not displacement within the cube volumes. Nevertheless, variation in displacement values indicates that there is relative movement within tracking points. Strain measurement removes this problem by providing an accurate description of local changes in displacement.

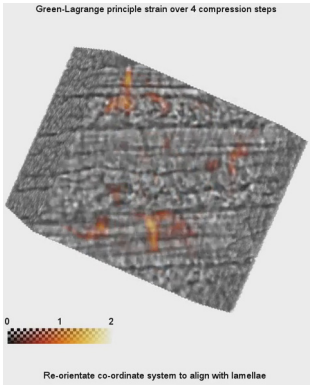

Video 4. Overview of the work in this paper is presented; i) A transverse slice shows the IVD structures resolved using synchrotron CT, ii) a medial cube volume of interest is selected and bundle analysis shown, iii) points are setup in the cube and sub-volume size is defined for displacement tracking using digital volume correlation, iv) after displacement of each point was found over all compression steps (4 x 2% strain), Lagrangian maximum principle strain and associated vectors were calculated and plotted with the image data.

Maximum principle strain and vectors, transformed to the local lamellae coordinate system, were calculated and mapped alongside the image data (Figs. 6 & 7). Overall the strain patterns are heterogeneous and not localised to lamellae boundaries. Vector components are displayed in a histogram to show overall strain values, where the medial cube (Fig. 6a) has areas of greater radial strain ($\varepsilon_{z'}$) than the lateral cube (Fig. 7a). Maximum principle strain appears to localise and span radially across several lamellae in a network at roughly 60 μm spacing. Maximum principle strain vectors for the lateral cube align with the collagen bundle structure (Fig. 7d & f).

4. Discussion

4.1. Novel 3D imaging of intact native IVD microstructure

Imaging of the disc in a spine segment was possible using synchrotron micro-tomography (synchrotron CT) as a non-destructive (without sectioning) technique. Different regions of the disc – endplate, NP and AF – have been identified (Fig. 1b). Naveh et al. [35] were also able to resolve these structures in native mouse IVD using laboratory μCT. In comparison, the synchrotron CT presented here clearly resolved the detailed AF hierarchical microstructure, such as lamellae bundles. Bundles could be traced in 3D which, to our knowledge, has not been achieved before. The NP appears to have a central region with higher grey values thought to be clustering of cells and there is some evidence of extra cellular matrix structure. Consistent with optical and MRI studies [30,52,53], fibres are organised from the centre radially outwards. These fibres are most evident in the vertical and anterior-to-posterior direction (Supplementary Fig. 1).

Yet, there are two observations to note. The calcified endplates are highly X-ray absorbing which reduced flux through the IVD and caused streaking artefacts. Additionally, NP contrast decreased after each compression step (Fig. 2b, Supplementary Video 1). This may be due to calcified material entering the beam path as the sample is compressed, increasing the severity of streaking artefacts and obscuring the NP. These artefacts are common in samples where sudden changes in X-ray absorption, such as metal implants [54], are observed. Image quality could be improved in future studies by removing the posterior elements which protrude from the vertebrae into the beam path and by carefully aligning the sample in the beam so that endplates run parallel with the beam.

Previous imaging studies which observed microstructure deformation were performed in 2D and required tissue dissection. Testing whole spine segments meant that the disc was maintained in its native physiological environment and loaded with the curved endplates. Furthermore, dissection of IVD tissue releases AF residual strain [21] which has regional variation, effecting bundle organisation [55,56]. Also, although MRI is capable of imaging intact samples, resolution is limited to ~200 μm which only allows for macro-scale strain analysis and quantification [9,29,57]. A recent ultrahigh field MRI study however achieved 100 μm resolution, resolving ovine lamellae bundles [30]. The higher synchrotron CT resolution presented here of ~5–6 μm, determined from the smallest resolved feature (bundle width), enabled resolution of rat IVD microstructure (Fig. 1d–f).

4.2. Lamellae bundle angle depends on anatomical position

Lamellae bundle angle has previously been shown to vary with circumferential position [10,13,58–60] but not radially towards the nucleus with the exception of a single dated study [14] and a recent study using ultrahigh field MRI of an intact disc [30] (Table 1). Fibre tracing image analysis showed that lamellae bundle angle varied from ±55–65° in the medial cube to ±25–30° in the lateral cube (Fig. 4c & f), which closely matches MRI diffusion characterisation from intact IVD [58].

The histograms in Fig. 4 do not show notable reorientation of collagen bundles after the spine segment is compressed. However, when average values from separate lamella are taken, the bundles reoriented by 0.9° ± 0.4°. This is in excellent agreement with previous studies that reported a similar value of bundles re-orientated during loading of around 1°/% strain and towards the orientation of the adjacent lamella [24,61].

4.3. Maximum principle strain

Importantly, the resolved microstructure provided sufficient image texture to track internal deformation using DVC (an overview of the process is presented in Supplementary Video 4). This is advantageous, as previous methods for imaging displacement in soft tissues required stains, dyed patterns or invasive markers [26,62,63] which can cause changes in tissue structure and

Please cite this article as: C. M. Disney, A. Eckersley, J. C. McConnell et al., Synchrotron tomography of intervertebral disc deformation quantified by digital volume correlation reveals microstructural influence on strain patterns, Acta Biomaterialia, https://doi.org/10.1016/j.actbio.2019.05.021

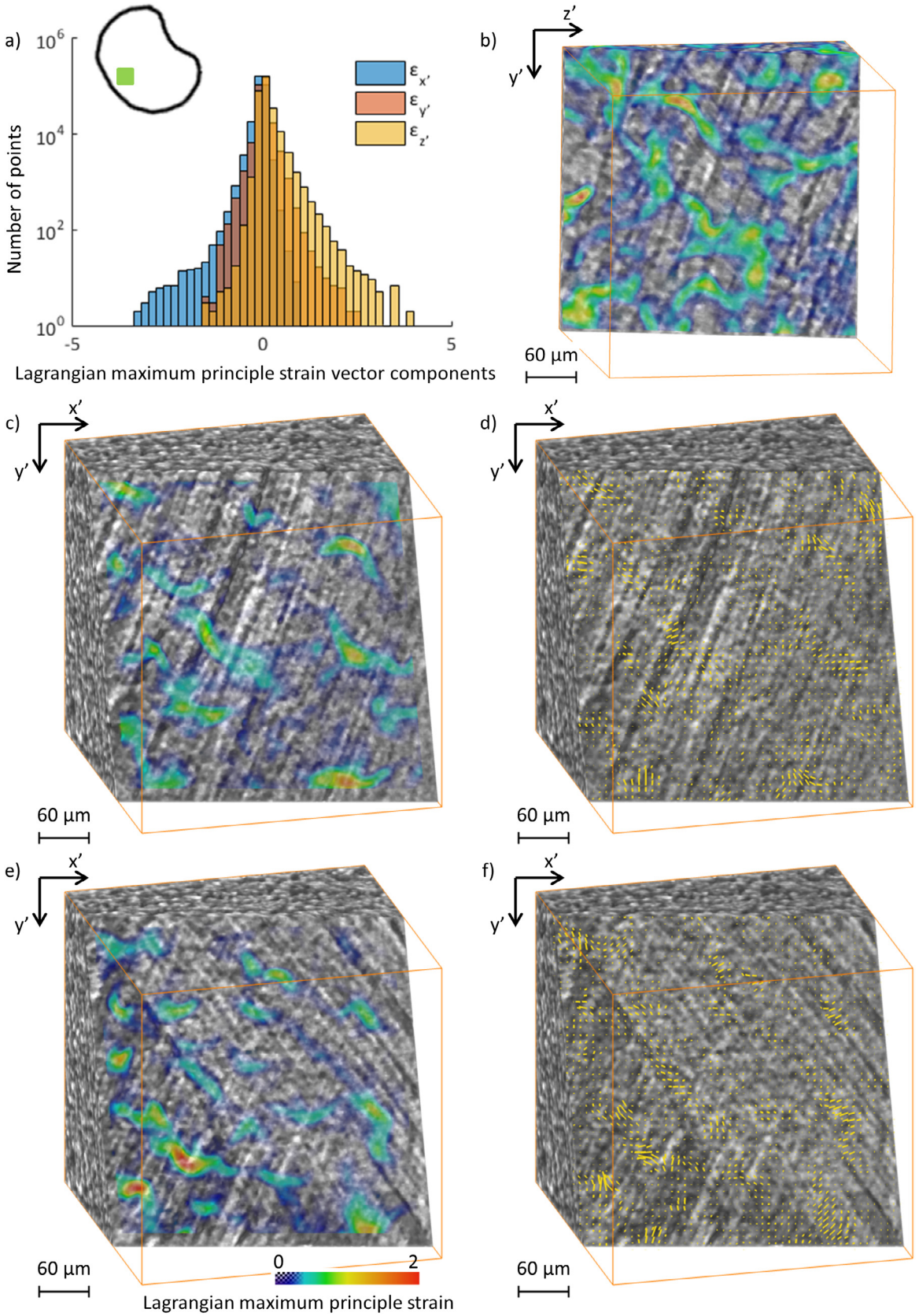

Fig. 6. Medial cube Lagrangian maximum principle strain: a) maximum principle strain vector components defined in local lamella coordinate system, b, c, e) maximum principle strain plotted with image data, clipped across lamella (b) and clipped in the lamella plane (c & e), and d & f) shows principle strain vectors in the lamella plane plotted with image data.

Please cite this article as: C. M. Disney, A. Eckersley, J. C. McConnell et al., Synchrotron tomography of intervertebral disc deformation quantified by digital volume correlation reveals microstructural influence on strain patterns, Acta Biomaterialia, https://doi.org/10.1016/j.actbio.2019.05.021

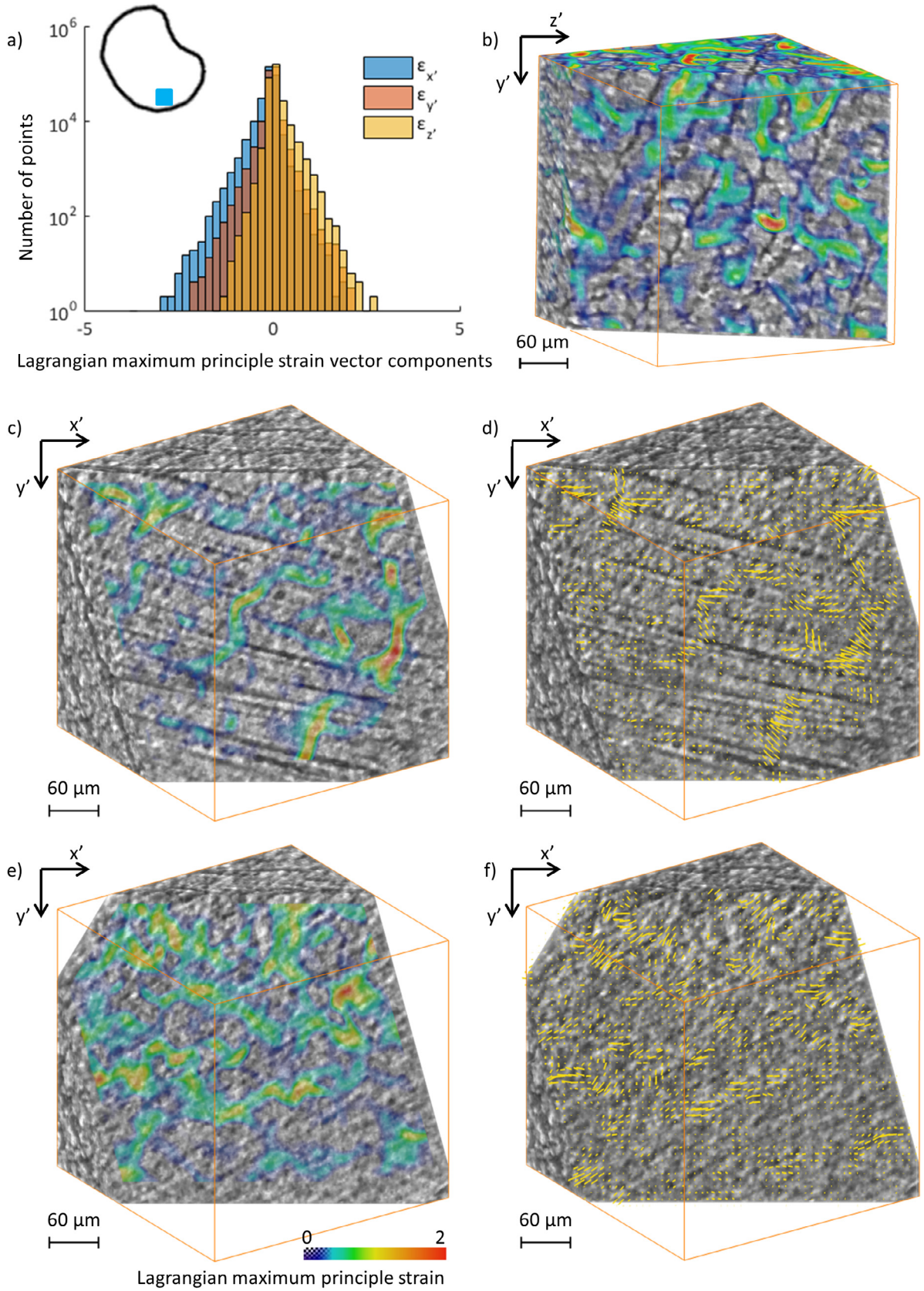

Fig. 7. Lateral cube Lagrangian maximum principle strain: a) maximum principle strain vector components defined in local lamella coordinate system, b, c, e) maximum principle strain plotted with image data, clipped across lamella (b) and clipped in the lamella plane (c & e), and d & f) shows principle strain vectors in the lamella plane plotted with image data.

Please cite this article as: C. M. Disney, A. Eckersley, J. C. McConnell et al., Synchrotron tomography of intervertebral disc deformation quantified by digital volume correlation reveals microstructural influence on strain patterns, Acta Biomaterialia, https://doi.org/10.1016/j.actbio.2019.05.021

Table 1
Lamella bundle angle from transverse plane has been shown to vary circumferentially. Most studies used dissection or lamella peeling and observation to measure bundle angle.

Bundle angle	Sample handling	Imaging method of measuring angle	Reference
28°–45° inward to nucleus	Dissection	Optical microscopy	[14]
Average 30°, posterior 70°	Lamella peeling and dehydration	Microscopic examination	[13]
23° ventral to 57° dorsal	Dissection	Photography	[60]
23° ventral to 47° dorsal	Lamella peeling	CCD camera analysis	[10]
25–30° front to 70–90° towards posterior ligament	Delamination	Photography	[59]
Ranged between 25° and 50°	Intact joint	MR diffusion	[58]
Ranged between 13° and 36° measured along radial depth	Intact joint	Ultrahigh field MRI	[30]
55–65° medial cube 25–30° lateral cube	Intact joint	Synchrotron CT	This study

mechanical behaviour [34,64]. In this study, full-field strain measurement is possible, which means that the local tissue strain can be observed when compared to the more global response from tracking markers.

Figs. 6 and 7 shows the maximum principle strain plotted alongside the image data for both cube volumes. Overall, the maximum principle strain pattern is heterogeneous throughout the local ECM without strain concentration at lamellae boundaries. These results support the conclusions of Michalek et al. [25] and Vergari et al. [24] who found that there was no slipping of the lamella boundary from direct confocal observations of AF tissue under load. It also provides further evidence against a disputed interpretation in an earlier study by Bruehlmann et al. [26] who suggested slipping at lamella boundary due to cells undergoing large motions in the interlamellar space. This is an example where tracking discrete markers can be misleading when compared to full-field strain measurement. Furthermore, discrete markers are not able to capture local in-homogenities as presented here and described by Spera et al. [65] who measured 3D surface deformation of an intact disc.

Maximum principle strain appears to be localised and traverse across lamellae in a network with spacing of ~60 μm. This pattern has a similar description to the AF shear strain inhomogeneities described by Han et al. [66]. In their study, there was strong strain localisation which is comparable to the results in Fig. 6 and Fig. 7. But, different spatial patterns may be present due to different loading modes (circumferential shear was applied by Han et al. [66]) and testing dissected tissue. The spatial pattern observed in Figs. 6 and 7 has some similarities to the elastic network distribution depicted by Tavakoli et al. [22,23] who suggest that this network is important for disc structural integrity. The illustration in Fig. 8 shows a highly integrated elastic network through the AF where elastic fibres are woven through collagen bundles and join and merge between the collagen bundles and lamellae. The inter lamellae dependency, shown by higher strain regions across multiple lamellae (Figs. 6b and 7b) and no slipping at the lamella boundary, relates well with the converging elastic network. Still, an improvement in imaging is required to confirm this. Therefore, we propose that the AF should be described as a multiscale fibre reinforced composite which includes both fibrous collagen and elastic fibre networks. The fibrous collagen bundles are acting as a composite fibre reinforcement phase, whereas the dense and interconnected elastic network is functioning as a matrix phase with low shear stiffness for flexibility and high strength to support loads. These are unique properties as it is unlikely that a non-fibrous biopolymer material would have this combination of properties.

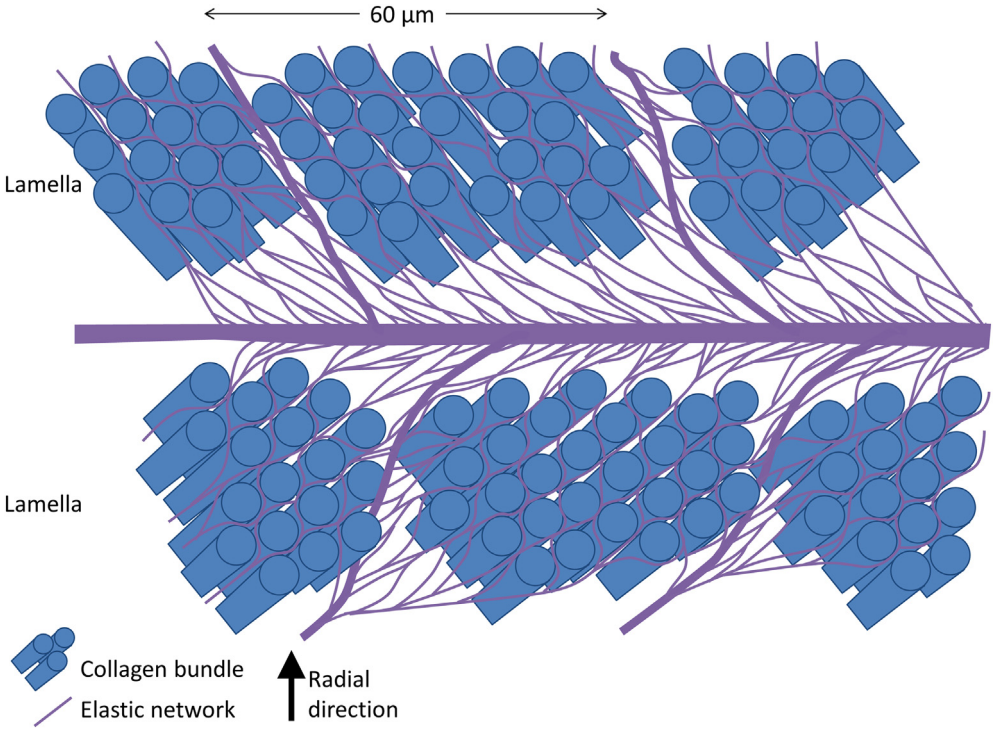

Fig. 8. Multiscale fibre organisation of the AF. A converging elastic network at bundle and lamella boundaries provides stability. Note that the elastic network illustrated here for visualisation is relatively sparse, and not to scale, when compared to imaging studies which show a much denser network encircling collagen bundles.

Please cite this article as: C. M. Disney, A. Eckersley, J. C. McConnell et al., Synchrotron tomography of intervertebral disc deformation quantified by digital volume correlation reveals microstructural influence on strain patterns, Acta Biomaterialia, https://doi.org/10.1016/j.actbio.2019.05.021

A comparison between the two cubes shows that there is regional variation in overall deformation mechanics. The medial cube has higher radial strain values when compared to the lateral cube (Figs. 6a and 7a). The maximum principle strain vectors are plotted alongside the image data in the lamella plane showing that their direction is aligned with bundle structure (Figs. 6d, f, and 7d, f). When strain direction was quantified, there was overall good alignment with the different bundle orientations for both cubes (Supplementary Fig. 2). It is encouraging to compare the results of these figures to several reports which showed that collagen fibrils un-crimped or stretched when load was applied to AF tissue segments [24–26]. Whilst fibrous collagen structures clearly have a mechanical role in the AF, proteoglycan-rich domains have been suggested to be responsible for heterogeneous strain patterns through the local ECM [67].

The results displayed in Figs. 6 and 7 show the cumulative strain from D0 to D4. To help demonstrate the validity of the analysis, strain data from the repeat scan at D0 and the intermediate results can be found in Supplementary Fig. 3 (tracking information in Fig. 5). It is reassuring that these intermediate results show a progression of increasing strain in both cubes. Supplementary Figs. 4 and 5 show maximum principle strain for the repeat scan at D0 plotted with the image data for both cubes (equivalent locations are taken as in Fig. 4.6 and 4.7). In comparison, the strain patterns displayed for the cubes at D0 appear to be similar to D4 but with a lower magnitude, this may be related to microstructural creep during the repeat scan time. Importantly, residual tracking error does not increase or change distribution through the compression sequence which indicates reliable tracking (Fig. 5c).

Note the advantages of taking measurements within the interior of intact samples when compared to surface observations of dissected tissue under load. The dissected samples from previous studies were not restrained by endplates or influenced by NP hydrostatic pressure which may have caused the AF to behave non-physiologically. Vergari et al. [24] described considerable transverse shrinkage of AF tissue without endplates during tensile loading. Furthermore, the applied uniaxial strain used in these studies could be greater than the strain present in the AF when an intact disc is compressed; for example, strain applied until failure [61].

4.4. Study limitations and future directions

It is important to bear in mind limitations of synchrotron CT. Firstly, synchrotron facilities can be accessed based on peer review application but are not as widely available as other imaging techniques. Secondly, the experiment is restricted to the beamline's capabilities. For example, rat lumbar spine samples were chosen to suit the beamline field of view and resolution. For a synchrotron (parallel) beam, field of view is ultimately restricted by the beam dimensions (largest field of view available at Diamond-Manchester Branchline is 14×9.6 mm). Additionally, a compromise between field of view and resolution has to be made. Although considerably smaller than a human IVD, the normalised IVD geometry of small animal models is close to human [68], particularly lumbar samples due to their limacon shape (concave at posterior surface) compared with circular tail geometry. Microstructural variation in collagenous tissue (such as thickness and number of lamellae) has been linked to the mechanical loads experienced *in vivo* [69] and so load magnitude must be suitable for that animal. IVD biomechanical properties are conserved across small animal models [70] and rat spine morphology has been shown as an appropriate model for axial loading of the human spine [71]. Furthermore, quadrupeds experience axial loads [72] caused by muscle and ligament constraining forces and also demonstrated by endplate to endplate organisation of the vertebrae trabeculae. Non-chondrodystrophoid models (pigs, rodents and some dogs) retain their notochord cells which are considered to be responsible for tissue repair and protecting against degeneration [73] but their effect on IVD micromechanics is not known.

The loading regime chosen was dependent on tissue relaxation and scan time. Shorter scan times limit the amount of slow tissue relaxation movement during the scan and so would enable a higher loading frequency. Scan time may be decreased in future studies by reducing image artefacts (through experiment set up or reconstruction methods) and therefore reducing the number of projections required. It is challenging to image the soft – calcified tissue interface due to variation in absorption of X-rays which, confounded by the phase contrast imaging mode used in this study, caused obscuring streaking artefacts. These artefacts can be reduced in future imaging by carefully positioning the sample in the beam.

Finally, imaging parameters must be carefully considered to compromise between image quality, reducing scan time and therefore minimising radiation dose. A filtered pink beam was used to reduce potential radiation damage. Although effects of radiation dose were not directly investigated, radiation damage was not apparent from the force curves which remained consistent throughout the experiment and strain patterns developed over the compression steps. Evidence of a decrease in vertebrae strength caused by radiation [74] such as microstructural changes or cracks were not observed.

A key strength of this study is that a native intact sample was tested. However, physiological loading of the disc, besides compression from weight bearing, is complex and includes torsion and bending for flexibility which when under dynamic conditions are known to cause damage to the disc [31,75,76]. More complex loading regimes will be important for future studies but may be challenged by the artefacts observed in this study.

5. Conclusions

The purpose of this study was to quantify IVD deformation within an intact spine segment. The 3D structure of the disc was resolved at microscale resolution using synchrotron CT which allowed measurement of bundle angle and supported digital volume correlation to track displacement of AF microstructure. This is the first study to directly image and trace AF bundles within an intact spine segment under compression, which will be of use to IVD mechanics research [77,78]. The strain analysis undertaken here builds on previous research in IVD experimental mechanics and imaging observations where: no slipping is observed at the lamella boundary [24,25], heterogeneous strain patterns can be observed throughout the local ECM [67] and strain localises to form a network similar to the distribution of the elastic network [22,23] and is aligned with bundle structure [24–26].

These methods provide a detailed insight into native IVD micromechanics and have the potential to bridge the gap between measures of macro-mechanical properties with the local 3D micromechanical environment experienced by cells. This study lays the groundwork for future research into: i) mechanical models which will be closer to IVD structure, ii) informing the design of potential tissue engineered IVD replacements and iii) evaluating the effects of surgical intervention on IVD mechanics. Beyond the IVD, it is likely that similar approaches could be employed to map 3D structure and strain within other non-calcified tissues.

Acknowledgements

The authors would like to gratefully acknowledge Sebastian Marussi for his assistance in adapting Deben CT5000 stage for this study and Research Complex at Harwell for laboratory facilities and equipment use.

Please cite this article as: C. M. Disney, A. Eckersley, J. C. McConnell et al., Synchrotron tomography of intervertebral disc deformation quantified by digital volume correlation reveals microstructural influence on strain patterns, Acta Biomaterialia, https://doi.org/10.1016/j.actbio.2019.05.021

C.M.D wrote the paper. C.M.D., B.K.B., M.J.S., P.D.L. and J.A.H. conceived and designed the study. C.M.D., A.E., J.C.M., H.G, A.J.B and M.J.S. collected the data. C.M.D. and B.K.B. contributed to the analysis and interpretation of the data. All authors contributed editing and final approval of the article.

Role of the funding source

C.M.D. was supported by an EPSRC & MRC Centre for Doctoral Training (CDT) Regenerative Medicine (EP/L014904/1) studentship and EPSRC Doctoral Prize Fellowship (EP/R513131/1). We gratefully acknowledge the Engineering and Physical Sciences Research Council (grants EP/I02249X/1, EP/M009688/1, EP/M022498/1). Facilities and research support were provided by the Diamond-Manchester Branchline (I13-2) and the Research Complex at Harwell. Diamond Light Source beam time was funded under proposal 15444 by the Diamond-Manchester Collaboration, with data analysis sessions at its associated data beamline [79]. Digital volume correlation code is supported by Collaborative Computational Project in Tomographic Imaging (CCPi) group (EP/M022498/1). These funding bodies were not involved in the study design, collection, analysis and interpretation of data, writing of the manuscript, or the decision to submit the manuscript for publication.

Competing financial interests

The authors have no conflicts of interests to declare.

Data availability

A representative sample of the data is provided in Supplementary material. Other datasets generated during and/or analysed during this study are not publicly available due to their large size but are available from the corresponding author on reasonable request.

Appendix A. Supplementary data

Supplementary data to this article can be found online at https://doi.org/10.1016/j.actbio.2019.05.021.

References

[1] D. Hoy, L. March, P. Brooks, F. Blyth, A. Woolf, C. Bain, G. Williams, E. Smith, T. Vos, J. Barendregt, The global burden of low back pain: estimates from the Global Burden of Disease 2010 study, Ann. Rheum. Dis. 73 (6) (2014) 968–974.
[2] K.M.C. Cheung, J. Karppinen, D. Chan, D.W.H. Ho, Y.-Q. Song, P. Sham, K.S.E. Cheah, J.C.Y. Leong, K.D.K. Luk, Prevalence and pattern of lumbar magnetic resonance imaging changes in a population study of one thousand forty-three individuals, Spine 34 (9) (2009) 934–940.
[3] P. Heindel, A. Tuchman, P.C. Hsieh, M.H. Pham, A. D'Oro, N.N. Patel, A.M. Jakoi, R. Hah, J.C. Liu, Z. Buser, J.C. Wang, Reoperation rates after single-level lumbar discectomy, Spine 42 (8) (2017) E496–E501.
[4] J.N. Weinstein, J.D. Lurie, T.D. Tosteson, A.N.A. Tosteson, E.A. Blood, W.A. Abdu, H. Herkowitz, A. Hilibrand, T. Albert, J. Fischgrund, Surgical versus nonoperative treatment for lumbar disc herniation four-year results for the spine patient outcomes research trial (SPORT), Spine 33 (25) (2008) 2789–2800.
[5] J. Tavakoli, J.J. Costi, New findings confirm the viscoelastic behaviour of the inter-lamellar matrix of the disc annulus fibrosus in radial and circumferential directions of loading, Acta Biomater. 71 (2018) 411–419.
[6] J.J. Costi, I.A. Stokes, M.G. Gardner-Morse, J.C. Iatridis, Frequency-dependent behavior of the intervertebral disc in response to each of six degree of freedom dynamic loading: solid phase and fluid phase contributions, Spine 33 (16) (2008) 1731.
[7] A. Race, N.D. Broom, P. Robertson, Effect of loading rate and hydration on the mechanical properties of the disc, Spine 25 (6) (2000) 662–669.
[8] J.C. Iatridis, L.A. Setton, M. Weidenbaum, V.C. Mow, The viscoelastic behavior of the non-degenerate human lumbar nucleus pulposus in shear, J. Biomech. 30 (10) (1997) 1005–1013.
[9] G.D. O'Connell, W. Johannessen, E.J. Vresilovic, D.M. Elliott, Human internal disc strains in axial compression measured noninvasively using magnetic resonance imaging, Spine 32 (25) (2007) 2860–2868.
[10] G.A. Holzapfel, C.A.J. Schulze-Bauer, G. Feigl, P. Regitnig, Single lamellar mechanics of the human lumbar anulus fibrosus, Biomech. Model. Mechanobiol. 3 (3) (2005) 125–140.
[11] D.M. Elliott, L.A. Setton, Anisotropic and inhomogeneous tensile behavior of the human anulus fibrosus: experimental measurement and material model predictions, J. Biomech. Eng. Trans. ASME 123 (3) (2001) 256–263.
[12] D.L. Skaggs, M. Weidenbaum, J.C. Iatridis, A. Ratcliffe, V.C. Mow, Regional variation in tensile properties and biochemical-composition of the human lumbar anulus fibrosus, Spine 19 (12) (1994) 1310–1319.
[13] F. Marchand, A.M. Ahmed, Investigation of the laminate structure of lumbar disc anulus fibrosus, Spine 15 (5) (1990) 402–410.
[14] J. Cassidy, A. Hiltner, E. Baer, Hierarchical structure of the intervertebral disc, Connect. Tissue Res. 23 (1) (1989) 75–88.
[15] S.K. Han, C.W. Chen, J. Wierwille, Y. Chen, A.H. Hsieh, Three dimensional mesoscale analysis of translamellar cross-bridge morphologies in the annulus fibrosus using optical coherence tomography, J. Orthop. Res. (2015).
[16] J. Yu, M.L. Schollum, K.R. Wade, N.D. Broom, J. Urban, A detailed examination of the elastic network leads to a new understanding of annulus fibrosus organisation, Spine (2015).
[17] G.D. O'Connell, E.J. Vresilovic, D.M. Elliott, Human intervertebral disc internal strain in compression: the effect of disc region, loading position, and degeneration, J. Orthop. Res. 29 (4) (2011) 547–555.
[18] D. McNally, M. Adams, Internal intervertebral disc mechanics as revealed by stress profilometry, Spine 17 (1) (1992) 66–73.
[19] A. Nachemson, The influence of spinal movements on the lumbar intradiscal pressure and on the tensile stresses in the annulus fibrosus, Acta Orthop. Scand. 33 (1–4) (1963) 183–207.
[20] D.C. Keyes, E.L. Compere, The normal and pathological physiology of the nucleus pulposus of the intervertebral disc: an anatomical, clinical, and experimental study, JBJS 14 (4) (1932) 897–938.
[21] A.J. Michalek, M.G. Gardner-Morse, J.C. Iatridis, Large residual strains are present in the intervertebral disc annulus fibrosus in the unloaded state, J. Biomech. 45 (7) (2012) 1227–1231.
[22] J. Tavakoli, J.J. Costi, Ultrastructural organization of elastic fibres in the partition boundaries of the annulus fibrosus within the intervertebral disc, Acta Biomater. 68 (2018) 67–77.
[23] J. Tavakoli, D.M. Elliott, J.J. Costi, The ultra-structural organization of the elastic network in the intra-and inter-lamellar matrix of the intervertebral disc, Acta Biomater. 58 (2017) 269–277.
[24] C. Vergari, J. Mansfield, J.R. Meakin, P.C. Winlove, Lamellar and fibre bundle mechanics of the annulus fibrosus in bovine intervertebral disc, Acta Biomater. 37 (2016) 14–20.
[25] A.J. Michalek, M.R. Buckley, L.J. Bonassar, I. Cohen, J.C. Iatridis, Measurement of local strains in intervertebral disc anulus fibrosus tissue under dynamic shear: contributions of matrix fiber orientation and elastin content, J. Biomech. 42 (14) (2009) 2279–2285.
[26] S.B. Bruehlmann, J.R. Matyas, N.A. Duncan, ISSLS prize winner: collagen fibril sliding governs cell mechanics in the anulus fibrosus: an in situ confocal microscopy study of bovine discs, Spine 29 (23) (2004) 2612–2620.
[27] C.M. Disney, P. Lee, J. Hoyland, M. Sherratt, B. Bay, A review of techniques for visualising soft tissue microstructure deformation and quantifying strain ex vivo, J. Microsc. (2018).
[28] M. Adams, D. McNally, P. Dolan, Stress'distributions inside intervertebral discs, J. Bone Joint Surg. Br. 78 (6) (1996) 965–972.
[29] D.D. Chan, C.P. Neu, Intervertebral disc internal deformation measured by displacements under applied loading with MRI at 3T, Magn. Reson. Med. 71 (3) (2014) 1231–1237.
[30] M. Sharabi, K.R. Wade, F. Galbusera, V. Rasche, R. Haj-Ali, H.-J. Wilke, Three-dimensional microstructural reconstruction of the ovine intervertebral disc using ultrahigh field MRI, Spine J. 18 (11) (2018) 2119–2127.
[31] N. Berger-Roscher, G. Casaroli, V. Rasche, T. Villa, F. Galbusera, H.-J. Wilke, Influence of complex loading conditions on intervertebral disc failure, Spine 42 (2) (2017) E78–E85.
[32] S. Bhalla, K.H. Lin, S.Y. Tang, Postnatal development of the murine notochord remnants quantified by high-resolution contrast-enhanced MicroCT, Sci. Rep. 7 (1) (2017) 13361.
[33] T. Maerz, M. Newton, K. Kristof, O. Motovylyak, J. Fischgrund, D. Park, K. Baker, Three-dimensional characterization of in vivo intervertebral disc degeneration using EPIC-μCT, Osteoarthritis Cartilage 22 (11) (2014) 1918–1925.
[34] C.M. Disney, K. Madi, A. Bodey, P. Lee, J. Hoyland, M. Sherratt, Visualising the 3D microstructure of stained and native intervertebral discs using X-ray microtomography, Sci. Rep. 7 (2017).
[35] G.R.S. Naveh, V. Brumfeld, M. Dean, R. Shahar, S. Weiner, Direct MicroCT imaging of non-mineralized connective tissues at high resolution, Connect. Tissue Res. 55 (1) (2014) 52–60.
[36] R.C. Atwood, A.J. Bodey, S.W. Price, M. Basham, M. Drakopoulos, A high-throughput system for high-quality tomographic reconstruction of large datasets at diamond light source, Philos. Trans. R. Soc. Lond. A: Math. Phys. Eng. Sci. 373 (2043) (2015) 20140398.
[37] S. Wilkins, T.E. Gureyev, D. Gao, A. Pogany, A. Stevenson, Phase-contrast imaging using polychromatic hard X-rays, Nature 384 (6607) (1996) 335.
[38] A. Snigirev, I. Snigireva, V. Kohn, S. Kuznetsov, I. Schelokov, On the possibilities of x-ray phase contrast microimaging by coherent high-energy synchrotron radiation, Rev. Sci. Instrum. 66 (12) (1995) 5486–5492.
[39] A. Momose, T. Takeda, Y. Itai, K. Hirano, Phase-contrast X-ray computed tomography for observing biological soft tissues, Nat. Med. (2) (1996) 473–475.

Please cite this article as: C. M. Disney, A. Eckersley, J. C. McConnell et al., Synchrotron tomography of intervertebral disc deformation quantified by digital volume correlation reveals microstructural influence on strain patterns, Acta Biomaterialia, https://doi.org/10.1016/j.actbio.2019.05.021

[40] B. Zeller-Plumhoff, J.L. Mead, D. Tan, T. Roose, G.F. Clough, R.P. Boardman, P. Schneider, Soft tissue 3D imaging in the lab through optimised propagation-based phase contrast computed tomography, Opt. Express 25 (26) (2017) 33451–33468.
[41] J. Tavakoli, D.M. Elliott, J.J. Costi, Structure and mechanical function of the inter-lamellar matrix of the annulus fibrosus in the disc, J. Orthop. Res. 34 (8) (2016) 1307–1315.
[42] N.L. Nerurkar, D.M. Elliott, R.L. Mauck, Mechanical design criteria for intervertebral disc tissue engineering, J. Biomech. 43 (6) (2010) 1017–1030.
[43] Z. Pešić, A. De Fanis, U. Wagner, C. Rau, Experimental stations at I13 beamline at diamond light source, J. Phys.: Conf. Ser. IOP Publ. (2013) 182003.
[44] C. Rau, U. Wagner, Z. Pešić, A. De Fanis, Coherent imaging at the diamond beamline I13, Phys. Status Solidi (a) 208 (11) (2011) 2522–2525.
[45] M.C. Strotton, A.J. Bodey, K. Wanelik, M.C. Darrow, E. Medina, C. Hobbs, C. Rau, E.J. Bradbury, Optimising complementary soft tissue synchrotron X-ray microtomography for reversibly-stained central nervous system samples, Sci. Rep. 8 (1) (2018) 12017.
[46] M. Basham, J. Filik, M.T. Wharmby, P.C. Chang, B. El Kassaby, M. Gerring, J. Aishima, K. Levik, B.C. Pulford, I. Sikharulidze, Data analysis WorkbeNch (DAWN), J. Synchrotron Radiat. 22 (3) (2015) 853–858.
[47] V. Titarenko, R. Bradley, C. Martin, P.J. Withers, S. Titarenko, Regularization methods for inverse problems in X-ray tomography, SPIE optical engineering + applications, Int. Soc. Opt. Photon. (2010). pp. 78040Z–78040Z-10.
[48] A. Rigort, D. Günther, R. Hegerl, D. Baum, B. Weber, S. Prohaska, O. Medalia, W. Baumeister, H.-C. Hege, Automated segmentation of electron tomograms for a quantitative description of actin filament networks, J. Struct. Biol. 177 (1) (2012) 135–144.
[49] B. Weber, G. Greenan, S. Prohaska, D. Baum, H.-C. Hege, T. Müller-Reichert, A.A. Hyman, J.-M. Verbavatz, Automated tracing of microtubules in electron tomograms of plastic embedded samples of Caenorhabditis elegans embryos, J. Struct. Biol. 178 (2) (2012) 129–138.
[50] B.K. Bay, Methods and applications of digital volume correlation, J. Strain Anal. Eng. Des. 43 (8) (2008) 745–760.
[51] B.K. Bay, T.S. Smith, D.P. Fyhrie, M. Saad, Digital volume correlation: three-dimensional strain mapping using X-ray tomography, Exp. Mech. 39 (3) (1999) 217–226.
[52] K.R. Wade, P.A. Robertson, N.D. Broom, On the Extent and Nature of Nucleus-Annulus Integration, Spine 37 (21) (2012) 1826–1833.
[53] J. Yu, C. Peter, S. Roberts, J.P. Urban, Elastic fibre organization in the intervertebral discs of the bovine tail, J. Anat. 6 (2002) 465–475.
[54] F.E. Boas, D. Fleischmann, Evaluation of two iterative techniques for reducing metal artifacts in computed tomography, Radiology 259 (3) (2011) 894–902.
[55] S.E. Duclos, A.J. Michalek, Mapping of intervertebral disc annulus fibrosus compressive properties is sensitive to specimen boundary conditions, J. Biomech. Eng. (2019).
[56] S.E. Duclos, A.J. Michalek, Residual strains in the intervertebral disc annulus fibrosus suggest complex tissue remodeling in response to in-vivo loading, J. Mech. Behav. Biomed. Mater. 68 (2017) 232–238.
[57] K.H. Lin, S.Y. Tang, The quantitative structural and compositional analyses of degenerating intervertebral discs using magnetic resonance imaging and contrast-enhanced micro-computed tomography, Ann. Biomed. Eng. 45 (11) (2017) 2626–2634.
[58] M.A. Stadelmann, G. Maquer, B. Voumard, A. Grant, D.B. Hackney, P. Vermathen, R.N. Alkalay, P.K. Zysset, Integrating MRI-based geometry, composition and fiber architecture in a finite element model of the human intervertebral disc, J. Mech. Behav. Biomed. Mater. 85 (2018) 37–42.
[59] D. Zhu, G. Gu, W. Wu, H. Gong, W. Zhu, T. Jiang, Z. Cao, Micro-structure and mechanical properties of annulus fibrous of the L4–5 and L5–S1 intervertebral discs, Clin. Biomech. 23 (2008) S74–S82.
[60] R. Eberlein, G.A. Holzapfel, C.A. Schulze-Bauer, An anisotropic model for annulus tissue and enhanced finite element analyses of intact lumbar disc bodies, Comput. Methods Biomech. Biomed. Eng. 4 (3) (2001) 209–229.
[61] H.A.L. Guerin, D.M. Elliott, Degeneration affects the fiber reorientation of human annulus fibrosus under tensile load, J. Biomech. 39 (8) (2006) 1410–1418.
[62] F. Fang, S.P. Lake, Multiscale strain analysis of tendon subjected to shear and compression demonstrates strain attenuation, fiber sliding, and reorganization, J. Orthop. Res. 33 (11) (2015) 1704–1712.
[63] S.E. Szczesny, D.M. Elliott, Interfibrillar shear stress is the loading mechanism of collagen fibrils in tendon, Acta Biomater. 10 (6) (2014) 2582–2590.
[64] S.E. Szczesny, R.S. Edelstein, D.M. Elliott, DTAF dye concentrations commonly used to measure microscale deformations in biological tissues alter tissue mechanics, PloS one 9 (6) (2014) e99588.
[65] D. Spera, K. Genovese, A. Voloshin, Application of stereo-digital image correlation to full-field 3-D deformation measurement of intervertebral disc, Strain 47 (2011) e572–e587.
[66] S.K. Han, C.-W. Chen, K.M. Labus, C.M. Puttlitz, Y. Chen, A.H. Hsieh, Optical coherence tomographic elastography reveals mesoscale shear strain inhomogeneities in the annulus fibrosus, Spine 41 (13) (2016) E770.
[67] W.M. Han, S.-J. Heo, T.P. Driscoll, L.J. Smith, R.L. Mauck, D.M. Elliott, Macro- to microscale strain transfer in fibrous tissues is heterogeneous and tissue-specific, Biophys. J. 105 (3) (2013) 807–817.
[68] G.D. O'Connell, E.J. Vresilovic, D.M. Elliott, Comparison of animals used in disc research to human lumbar disc geometry, Spine 32 (3) (2007) 328–333.
[69] D.F. Holmes, Y. Lu, T. Starborg, K.E. Kadler, Collagen fibril assembly and function, Curr. Top. Dev. Biol. Elsevier (2018) 107–142.
[70] J.C. Beckstein, S. Sen, T.P. Schaer, E.J. Vresilovic, D.M. Elliott, Comparison of animal discs used in disc research to human lumbar disc: axial compression mechanics and glycosaminoglycan content, Spine 33 (6) (2008) E166–E173.
[71] N.V. Jaumard, J. Leung, A.J. Gokhale, B.B. Guarino, W.C. Welch, B.A. Winkelstein, Relevant anatomic and morphological measurements of the rat spine, Spine 40 (20) (2015) E1084–E1092.
[72] S. Reitmaier, H. Schmidt, R. Ihler, T. Kocak, N. Graf, A. Ignatius, H.-J. Wilke, Preliminary investigations on intradiscal pressures during daily activities: an in vivo study using the merino sheep, PLoS One 8 (7) (2013).
[73] D.J. Aguiar, S.L. Johnson, T.R. Oegema Jr, Notochordal cells interact with nucleus pulposus cells: regulation of proteoglycan synthesis, Exp. Cell Res. 246 (1) (1999) 129–137.
[74] S.R. Emerzian, M.M. Pendleton, A. Li, J.W. Liu, J.S. Alwood, G.D. O'Connell, T.M. Keaveny, Effect of Ex Vivo Ionizing Radiation on Static and Fatigue Properties of Mouse Vertebral Bodies, 2018. NTRS 20180001896.
[75] H.-J. Wilke, A. Kienle, S. Maile, V. Rasche, N. Berger-Roscher, A new dynamic six degrees of freedom disc-loading simulator allows to provoke disc damage and herniation, Eur. Spine J. 25 (5) (2016) 1363–1372.
[76] K.R. Wade, P.A. Robertson, A. Thambyah, N.D. Broom, How healthy discs herniate a biomechanical and microstructural study investigating the combined effects of compression rate and flexion, Spine 39 (13) (2014) 1018–1028.
[77] A. Malandrino, J. Noailly, D. Lacroix, Numerical exploration of the combined effect of nutrient supply, tissue condition and deformation in the intervertebral disc, J. Biomech. 47 (6) (2014) 1520–1525.
[78] J. Noailly, J.A. Planell, D. Lacroix, On the collagen criss-cross angles in the annuli fibrosi of lumbar spine finite element models, Biomech. Model. Mechanobiol. 10 (2) (2011) 203–219.

Please cite this article as: C. M. Disney, A. Eckersley, J. C. McConnell et al., Synchrotron tomography of intervertebral disc deformation quantified by digital volume correlation reveals microstructural influence on strain patterns, Acta Biomaterialia, https://doi.org/10.1016/j.actbio.2019.05.021